



Enforcing conservation of axial angular momentum in
the atmospheric general circulation model CAM6

Thomas Toniazzo^{1,2}
Mats Bentsen¹
Cheryl Craig³
Brian Eaton³
James Edwards³
Steven Goldhaber³
Christiane Jablonowski⁴
Peter J. Lauritzen³

¹NORCE Klima and Bjerknes Centre for Climate Research, Bergen, Norway

²Department of Meteorology (MISU), Stockholm University, Stockholm, Sweden

³National Center for Atmospheric Research, Boulder, Colorado, USA

⁴University of Michigan, Ann Arbor, Michigan, USA

- 1 Corresponding author's address:
- 2 Thomas Toniazzo
- 3 NORCE Research AS
- 4 Bjerknes Centre for Climate Research
- 5 Geophysical Institute, Jahnebakken 5
- 6 Bergen, Hordaland, Norway NO-5070
- 7 e-mail: thomas.toniazzo@uni.no



8

Abstract

9 We present a numerical method to enforce global conservation of atmospheric axial
10 angular momentum (AM) in the Community Atmosphere Model (CAM). We discuss the
11 results in a hierarchy of numerical simulations of the atmosphere of increasing complexity,
12 and we demonstrate the importance of global AM conservation in climate simulations.

13 1 Introduction

14 The atmosphere exchanges angular momentum (AM) with the material bodies at the surface
15 which are, to a good approximation, in a state of motion consisting in uniform rotation about
16 the planetary axis connecting the poles. Per unit of mass, surface specific AM increases in
17 quadratic proportion to its distance from the planetary axis of rotation, from zero at the poles
18 to a maximum at the Equator. As atmospheric air travels meridionally, it carries a specific AM
19 that increasingly differs from that at the surface, which results in an exchange of AM between
20 the atmosphere and the surface by a variety of mechanisms. The most important of these are
21 turbulent stresses generated by low-level wind shear (“surface stress”) and by small-scale wave
22 motions over steep surface topography (“form drag”).

23 The importance for the atmospheric circulation of conservation of AM in the free troposphere
24 and of AM exchange of air with the surface was recognised long ago. Already in 1735, George
25 Hadley, Esq, F.R.S., noted that without the Assistance of the diurnal Motion [i.e. rotation] of
26 the Earth, Navigation [...] would be very tedious (Hadley 1735), due to the absence of the trade
27 winds. This insight still lies at the core of modern conceptual models for the atmospheric circu-
28 lation (Schneider, 1977; Held and Hou, 1980; Lindzen and Hou, 1988; Pauluis, 2004; Walker and
29 Schneider, 2006). In the upper branch of the Hadley Circulation (HC), the advection of plane-
30 tary angular momentum determines a sharp acceleration of the zonal wind in the mid-latitudes,
31 linked with a front-like drop in air temperatures, marking the location of the subtropical jets
32 (STJs). As a result of baroclinic instability, air loses AM in the mid-latitude surface Westerlies.
33 The equatorward return flow in the surface branch of the HC generate the trade winds, where
34 surface stresses replenish atmospheric AM until air is lifted in cumulus convection within the
35 inter-tropical convergence zone (ITCZ).

36 This circulation is the object of numerical simulations with general circulation models (GCMs)
37 used in meteorological forecasting and in climate modelling. They describe the atmosphere as
38 a thin, density-stratified, rotating gaseous spherical shell. These properties allow the introduc-
39 tion of a convenient set of approximations in the equations of motion, which result in a system



40 known as the Hydrostatic Primitive Equations (HPEs). The reader is referred to White et al.
41 (2005) for a detailed analysis and discussion. Given suitable boundary conditions, the HPEs
42 guarantee the global conservation of three fundamental physical quantities: mass; energy; and
43 AM along the Earth's rotation axis. Analytic expressions of these laws can be found e.g. in
44 Laprise and Girard (1990). The three conservation laws determine the fundamental character of
45 the large-scale circulation of the atmosphere, and virtually every climate application of GCMs is
46 sensitive to their enforcement when the continuum equations are discretized in space and time.
47 For example, the effects of changes in radiative forcing of 2 W/m^2 (e.g. IPCC AR5, Chapter
48 8, pg 697) can only be simulated if the model's energy conservation is significantly better than
49 1%. Estimates based on ECMWF reanalysis data suggest that conservation of AM of a similar
50 precision is desirable for an accurate representation of the annual cycle and of interannual
51 variations of the atmospheric circulation in model simulations (e.g. Egger and Hoinka 2005).

52 CAM, the Community Atmosphere Model developed and maintained at the National Center
53 for Atmospheric Research (NCAR) in Boulder, Colorado, is one of the Atmospheric General
54 Circulations Models (AGCM) in most widespread use today. It also constitutes the core atmo-
55 spheric component of NorESM, the Norwegian Earth System Model. Although it offers a choice
56 of dynamical cores, the finite-volume (FV) dynamical core (Lin 2004) has been, and in many
57 instances still is, the default option. It has been employed in all model integrations submit-
58 ted by NCAR and by the Norwegian Climate Centre (NCC) for the 5th phase of the Coupled
59 Model Inter-comparison Project (CMIP) contributing to the Assessment Report (AR) of the
60 Intergovernmental Panel for Climate Change (IPCC 2013); it is also expected to be used for
61 phase 6th of CMIP by both institutions. Due to its high numerical efficiency, FV also continues
62 to be the code of choice for all uses where overall availability of supercomputing resources is a
63 limiting factor. This includes long historical or palaeoclimate simulations; studies with coupled
64 chemistry and/or carbon cycle; seasonal-to-decadal coupled forecasts; academic research; and
65 all model development efforts currently underway with NorESM.

66 In agreement with previous results (Lauritzen et al., 2014; Lebonnois et al., 2012), we find
67 that all existing simulations with CAM FV, from CMIP5 to present development versions of
68 CAM6, have a numerical sink of global AM of a magnitude of about 30% of physical sources at
69 $1.9^\circ \times 2.5^\circ$ resolution ("f19" for short), and about 15% at $0.9^\circ \times 1.25^\circ$ ("f09") resolution.

70 Figure 1 shows the spurious AM source in aquaplanet (AP; Neale and Hoskins, 2000; Black-
71 burn et al., 2013) and Held-Suarez (HS; Held and Suarez 1994) simulations with CAM FV, and
72 an AP case with the Eulerian grid at T42 truncation for comparison. Although many other



73 models also do not conserve AM, CAM FV is peculiar in producing a sink nearly everywhere,
 74 resulting in a particularly large global non-conservation.

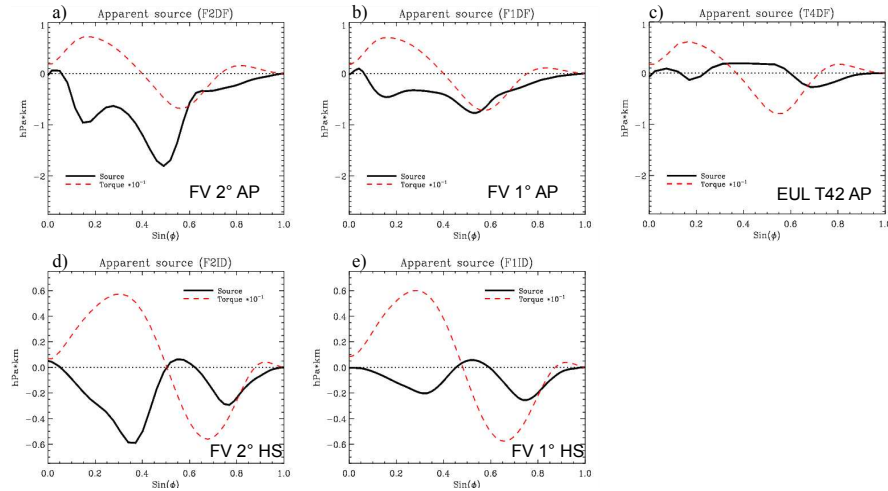


Figure 1: Numerical torque in idealised CAM simulations. The vertically and zonally integrated apparent numerical torque is shown as a function of latitude for CAM simulations in Aquaplanet (AP; panels a, b) and c) in the top row) and Held-Suarez (HS; panels d) and e) at the bottom) configurations. The numerical torque here is obtained as a time-average residual of the tendency of angular momentum in each cylindrical shell of constant latitude of the model’s domain, after subtracting the contributions from meridional convergence and from the surface stress torque. The details of the calculation are in Appendix A. Two simulations with the FV dynamical core are shown for each configuration, one with on a regular latitude-longitude grid with spacing of $1.9^\circ \times 2.5^\circ$ (panels a) and d)), and one with twice that resolution (panels b) and e)). For comparison, also a CAM simulation in AP configuration with the global spectral dynamical core at quadratic triangular truncation T42 (roughly comparable to FV at $1.9^\circ \times 2.5^\circ$ resolution) is shown in panel c). The dashed red line in each panel indicate the physical torque from surface stresses, scaled by a factor 0.1. Positive values indicate an eastward torque acting on the atmosphere, and negative values indicate a westward torque acting on the atmosphere.

75 First principles (e.g. Held and Hou, 1980; Einstein, 1926) suggest that dissipation of AM,
 76 equivalent to a body force acting on the fluid as a sink of zonal momentum, forces a secondary
 77 circulation with the same sign as the Hadley circulation. As a result, the simulated Hadley
 78 circulation may become too vigorous. Reduced meridional advection of zonal momentum may
 79 lead to mid-latitude Westerlies that are too weak or displaced poleward. The zonal momentum
 80 lost to the non-physical sink must be balanced by a matching additional eastward torque, for
 81 example in an expanded or excessively intense area of tropical easterly surface winds. Model



82 simulations with CAM FV consistently tend to reflect such phenomenology: for example, Feldl
83 and Bordoni (2016) and Lipat et al. (2017) show that among CMIP5 models, those based
84 on the FV dynamical core (GFDL-x, CCSM4 and NorESM-x) simulate both relatively large
85 overturning mass flux in the HC, and a high latitude of its edge.

86 It is useful to illustrate these effects of AM non-conservation by means of idealised AGCM ex-
87 periments that do not include complicating factors such as orographic form drag or parametrised
88 bulk stresses associated with gravity waves. Figure 2 shows the surface torques resulting from
89 four solutions for the mean circulation with CAM in AP mode. One of these is obtained directly
90 from integrations of CAM using the FV dynamical core at f19 resolution (black line). An oth-
91 erwise identical integration with the global spectral-transform dynamical core at T42 spectral
92 truncation (green line) is chosen for comparison as a bone-fide example of an AM conserving
93 simulation (cf Figure 1).

94 The other two integrations, represented by the blue and red lines, are perturbed in identical,
95 but opposite manner. First, the global-total numerical torque due to the FV dynamical core was
96 diagnosed at every time-step of the reference FV simulation, and averaged in time afterwards.
97 This was converted into a solid-body axial rotation tendency that was applied continuously
98 everywhere as a constant sink of AM in a new integration with the spectral dynamical core,
99 resulting in the simulation represented by the red curve. Vice-versa, the opposite additional
100 solid-body rotation tendency was applied to a new FV integration, thus compensating its internal
101 numerical sink. This integration produced the physical torque represented by the blue curve.
102 Comparing the different curves, it may be seen that Equatorward of about 23 degrees of latitude
103 the simulated physical torque depends primarily on the global budget of atmospheric AM. In
104 particular, notwithstanding the complications of interactive moist physics and the different
105 spatial and temporal discretisations used in the two integrations, the stronger trade winds
106 (in terms of surface stress) in the FV simulation compared with the T42 simulation can be
107 explained entirely with the non-physical, numerical torque of the FV dynamical core. The
108 result is insensitive to how that torque is in fact applied. Even at subtropical and middle
109 latitudes, half of the difference between the two simulations, in terms of surface stresses, can be
110 explained in this way. Similar results are found for the zonal-mean meridional circulation and
111 for the surface pressure in the HC (Figure S1 in the Supplementary Information), confirming
112 the strength and robustness of the Einstein (1926) “tea-leaves” mechanism.

113 These results motivate us to address the issue of AM conservation in the CAM’s FV dynam-
114 ical core. One may speculate that systematic biases in surface stresses due to the numerical sink

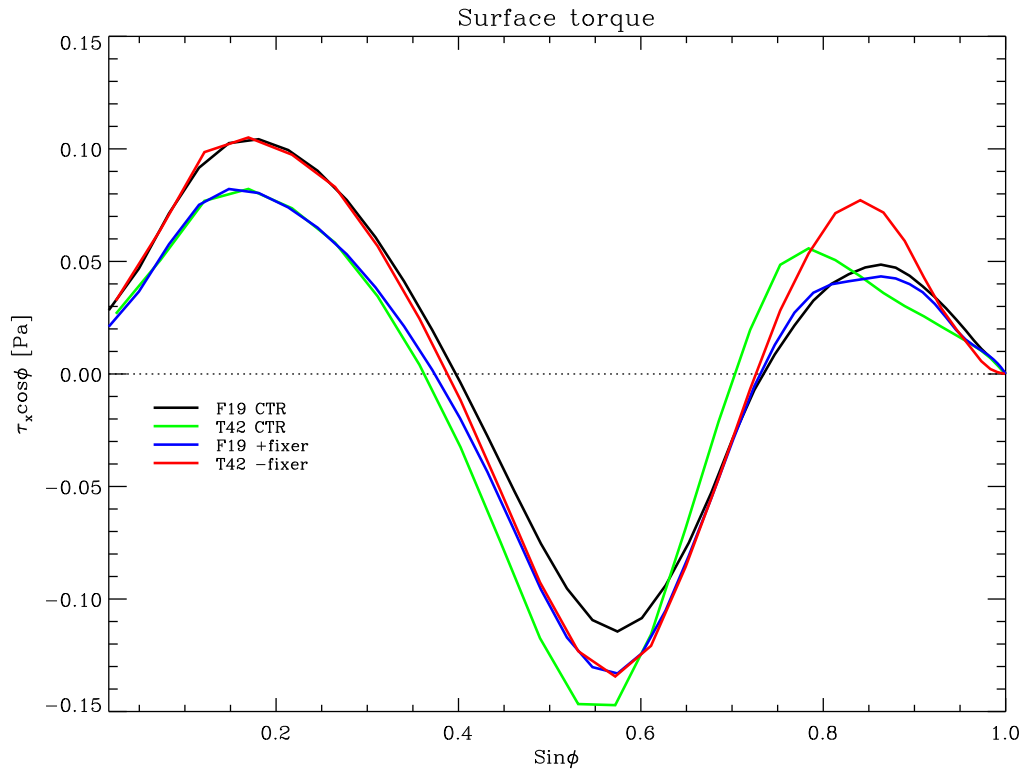


Figure 2: Impact of AM sink in CAM-FV integrations. Meridional distribution of the surface stress torque (analogous to the dashed red lines in Figure 1) in CAM simulations in AP configuration. Two integrations with the FV dynamical core (black and blue lines), and two simulations with the global spectral dynamical core (green and red lines) are shown. One of each pair of integrations is a control case (black and green lines), the other (blue and red lines) is an experiment where an additional solid-body angular acceleration is applied to the entire atmosphere at each time-step of the integration. The acceleration is diagnosed as the time mean of the ratio between the global total numerical torque in the FV control integration and the moment of inertia of the atmosphere. That acceleration is then applied with a negative sign in the FV experiment (blue curve), with the effect of compensating for the numerical torque and achieving approximate global AM conservation in that integration. For the experiment with the spectral dynamical core (red curve), the acceleration is applied with unchanged sign, causing a sink of AM approximately equal to that of the control FV integration. The numerical sink of the control spectral integration is nearly vanishing.

115 of AM must also impact coupled ocean-atmosphere climate simulations, with excessive Ekman
 116 and Sverdrup forcing of the subtropical gyres. The northward displacement of the mid-latitude



117 westerlies may also result in excessive mechanical and thermal forcing of the subpolar gyres with
118 possible implications for the Atlantic meridional overturning circulation.

119 In this paper, we propose ways to address numerical dissipation of AM in CAM-FV sim-
120 ulations. Section 2 describes our main hypotheses as to the root cause of the error, and our
121 approaches towards rectification. Section 3 presents the result of our corrections in a set of
122 idealised simulations. The impact on realistic simulations of the atmospheric circulation is
123 discussed in Section 4. Conclusions are finally offered in Section 5.

124 **2 Analysis of potential causes and approaches to correc-** 125 **tion.**

126 The FV dynamical core (Lin 2004) solves the HPE by updating first the advective (C-grid)
127 and then the prognostic (D-grid) winds in two steps. The first step represents pure advection,
128 i.e. the increments associated with transport, including geometric and Coriolis terms. In this
129 step, the scheme conserves absolute vorticity exactly for the D-grid winds (Lin and Rood 1997;
130 hereafter LR97). The second step calculates the wind increments associated with hydrostatic
131 pressure forces. These are computed in a special way (Lin 1997) that differs from most Arakawa
132 and Lamb (1980) type schemes. Violations of AM conservation may occur in either step.

133 **2.1 Pressure-gradient force**

134 We first analysed the Lin's (1997) treatment of the pressure-gradient terms for conservation. A
135 general discussion is given by Simmons and Burridge (1980), who introduce a set of hybrid-level
136 dimensionless variables, a_k , defined as $a_k := (\phi_k - \phi_{k+1/2})/2(\alpha p)_k$ (in Simmons and Burridge
137 these variables are denoted by α_k ; we change the notation here to avoid confusion), where ϕ is the
138 geopotential, p the pressure, and $\alpha := -\partial_\eta \phi / \partial_\eta p$ the specific volume. The index k refers to the
139 vertical level, or to half-levels as appropriate. The variables a_k need not be constants. Simmons
140 and Burridge (1980) derive the discrete form that pressure and geopotential terms must take in
141 general vertical coordinates in order to ensure conservation of axial angular momentum. Their
142 Equation (3.8) can be generalised to:

$$(\alpha \partial_\lambda p + \partial_\lambda \phi)_k = - \left(\frac{\Delta \phi}{\Delta p} \right)_k \partial_\lambda p_{k-1/2} + \partial_\lambda \phi_{k+1/2} + \frac{1}{\Delta p_k} \partial_\lambda [a_k (\alpha p)_k \Delta p_k] , \quad (1)$$

143 where $\Delta p_k := p_{k+1/2} - p_{k-1/2}$ (and similarly for ϕ).



144 Performing Lin's (1997) path integration around the finite-volume element on this expression
145 yields the following form for the body force:

$$\oint \phi dp = \delta_\lambda \{ [\phi_{k+1/2} + a_k(\alpha p)_k] \Delta p_k \} - \Delta (\overline{\phi \delta_\lambda p})_k \quad (2)$$

146 where δ_λ is the finite-difference operator in the zonal direction, and $\overline{\phi_{k\pm 1/2}}$ is an average over λ .
147 An expression identical in form to Lin's (1997) Equation (11) is then recovered if the choices

$$a_k = \frac{\Delta_k}{2(\alpha p)_k}, \quad \overline{\phi} = \frac{\phi_{\lambda+1/2} + \phi_{\lambda-1/2}}{2}, \quad (3)$$

148 are made.

149 In other words, Lin's (1997) expression for the pressure-gradient term is consistent with
150 Simmons and Burridge (1980) prescription for AM conservation, provided that the physical
151 pressure variable p is used in the integration in place of the general pressure function indicated
152 be the symbol π in Lin (1997). This can be directly verified algebraically by summing all
153 expressions of the form of the numerator in the right-hand side of Equation (11) in Lin (1997)
154 along all longitudes and levels. Provided ϕ is constant at one model boundary, and p at the other,
155 it always returns zero. This is the required result provided that the denominators represent the
156 inertia associated with the velocity points. They do if π is the hydrostatic pressure.

157 Accordingly, we performed tests in which the integration variable in the relevant section of
158 CAM-FV's dynamical core was replaced with true interface pressure. The effect was generally
159 seen to be very small on the dynamical core's momentum conservation properties.

160 We note however that in the CAM implementation there may be an additional problem,
161 associated with the use of the D-grid. The application of Lin's (1997) method would strictly
162 require a C-grid, with zonal velocity points interleaving pressure (scalar) points along the same
163 latitude. Thus, in CAM pressure is interpolated to the grid-cell corners before use. While the
164 formal expressions for the pressure forces do not change, thus ensuring S&B's total torque con-
165 straints, the inertia associated with each D-grid U -point is in fact averaged over six scalar point
166 surrounding it, with 1-2-1 weights along the zonal direction. This additional zonal smoothing
167 effectively adds spurious terms to the zonal momentum equation, of the form $-u\partial_x^2\Delta p$. This is
168 a potential source of non-conservation. However, it is not expected to be systematic.

169 2.2 Geometry, polar filtering, and FFSL extension

170 AM conservation may be affected by the treatment of geometric terms in latitude-longitude
171 coordinates, especially near the poles where such terms become large. Furthermore, convergence



172 of the meridians forces filtering of the solution, and additional approximations to be made. In
173 particular, LR97 implement a flux-form semi-Lagrangian extension of Colella and Woodward’s
174 (1984) PPM algorithm which is used near the poles where CFL numbers become large during
175 the time integration. We performed several sensitivity tests on each of these aspects, without
176 being able to notice significant impacts on AM conservation.

177 Particularly compelling is the comparison with the performance of a prototype implementa-
178 tion in CAM of the FV scheme on a cubed-sphere grid (“FV3”), which lacks any poles and does
179 not require or use any of these special formulation (and is, in particular, run in pure Eulerian
180 mode). We ran an AP simulation on the C48 grid, viz. six pseudo-cubic faces with 48x48 grid-
181 cells each, for total number of grid-points identical to the standard 2-degree FV configuration,
182 but a 25% higher resolution at the Equator. The AM sink (Figure S2 in the Supplementary
183 Information) is nevertheless comparable, i.e. about 25% smaller, consistently with the scaling
184 with the resolution of simulations with standard FV. We conclude that FV and FV3 suffer from
185 the same problem, independent of geometry or the FFSL extension of LR97.

186 In order to minimise the impact of other minor (and partly intentional) numerical sources
187 and sinks of AM, in all idealised numerical tests presented in this paper we applied the following
188 modifications: 1. the order of the advection scheme is kept the same (4th) for all model layers,
189 instead of reducing it to 1st in the top layer and to 2nd up to the 8-th layer; 2. an additional
190 conservation check is applied in the vertical remapping of zonal wind and column momentum
191 is conserved in the moist-mass adjustment at the end of physics; 3. the surface-stress residual
192 resulting from closure of the diffusion operator (in physics) is applied in full rather than partially.

193 **2.3 Discretisation of the kinetic-energy term**

194 The evidence from our theoretical and diagnostic analysis points at the advective, shallow-water
195 part of the implementation of LR97 in CAM-FV as the root of the AM conservation error.
196 Its ”vector-invariant” formulation (Arakawa and Lamb 1981) allows for different forms of the
197 divergence to be used in the momentum and in the mass and tracer equations, resulting in
198 inconsistent values for the divergence of the planetary AM (associated with mass divergence)
199 and of the relative AM (associated with momentum divergence). In the momentum equations,
200 the divergence is contained in a kinetic-energy (KE) gradient term, which due to the presence of
201 a numerical symmetric instability (Hollingsworth et al., 1983) is expressed as the local gradient
202 of a Lagrangian-average KE. Its form violates the finite-volume approximations used for other
203 quantities, e.g. vorticity. This feature is intrinsic to the LR97 numerical discretisation scheme



204 and cannot be eliminated.

205 To address the problem, we first note that even in AM-conserving schemes, conservation can
 206 only be guaranteed in the zonal average (Simmons and Burridge, 1980). We therefore do not
 207 attempt a local correction to the scheme, which is liable to numerical instabilities (Hollingworth
 208 et al., 1983), and instead formulate a zonal-mean correction as follows. We enforce the AM
 209 conservation law:

$$\int d\lambda \partial_t (\Delta p u a \cos^2 \varphi) = - \int d\lambda \partial_\varphi (\Delta p u v \cos^2 \varphi) + \int d\lambda \Delta p f v a \cos^2 \varphi \quad (4)$$

210 by adding a zonal-mean zonal-wind tendency term to the "vector-invariant" form:

$$\begin{aligned} \partial_{t,c} \bar{u} &= \frac{1}{\int d\lambda \Delta p} \\ &\times \left\{ \int d\lambda \Delta p \left(\frac{1}{a \cos \varphi} \partial_\lambda K - \zeta v \right) - \int d\lambda \frac{1}{a \cos^2 \varphi} \partial_\varphi (\Delta p u v \cos^2 \varphi) - \int d\lambda u \partial_t \Delta p \right\}. \end{aligned} \quad (5)$$

211 Here, K is the KE plus the contribution from explicit divergence damping used in FV. In the
 212 continuum limit the expression on the right-hand side reduces simply to the mass-weighted zonal
 213 average of the zonal gradient of $K - (u^2 + v^2)/2$.

214 In discrete form, the last two terms must be approximated. In the C-D grid formulation of
 215 the LR97 scheme the second one is especially problematic. Various possibilities were explored,
 216 which resulted in various degrees of accuracy and stability. The best compromise is to discretise
 217 it as

$$\frac{1}{a \cos^2 \varphi} \partial_\varphi (\Delta p u v \cos^2 \varphi) = \frac{1}{a \cos^2 \varphi} [\Delta p v \partial_\varphi (u \cos \varphi) + u \partial_\varphi (v \Delta p \cos \varphi)], \quad (6)$$

218 allowing some confusion between prognostic D-grid winds and time-centred advective (C-grid)
 219 winds. The details of the derivation are given in Appendix A. Using the mass conservation
 220 equation, this approximation allows us to discretize the two last terms together and write the
 221 zonal-wind correction increment in a form consistent with LR97:

$$\delta_c \bar{u} = \frac{1}{\int d\lambda \overline{\Delta p_{t+\delta t}}} \left\{ \int d\lambda \overline{\Delta p} \left[\frac{\delta t}{a \cos \varphi \delta \lambda} \delta_\lambda K - \overline{\mathcal{Y}(v^*, \delta t; \zeta_\lambda)} \right] + \bar{u}^t \mathcal{F}(u^*, \delta t; \overline{\Delta p}) + O(\delta t^2) \right\}, \quad (7)$$

222 where the notation of LR97 is used for the operators \mathcal{Y} and \mathcal{F} , $\zeta_\lambda := \frac{1}{a \cos \varphi} \partial_\lambda v$, and the last
 223 symbol on the right-hand side represents higher-order terms (see Appendix A). We will refer to
 224 this modification of the LR97 scheme as the "correction".



225 2.4 Diagnostic tools and global conservation

226 Irrespective of whether the correction, as described above, is applied or not, for diagnostic pur-
227 poses we calculate the apparent non-physical torque associated with the FV dynamical core
228 advective tendencies only, i.e. excluding the increments associated with pressure gradients.
229 These tendencies are diagnosed separately for each layer at every dynamic sub-step, and inte-
230 grated horizontally to yield the apparent numerical global-total torque during the sub-step. At
231 the same time, the layer effective moment of inertia over the sub-step is also computed.

232 The opposite of the ratio of these quantities gives an angular acceleration, representing
233 the solid-body rotation increment that, applied to the zonal wind in each layer at every sub-
234 step, is required in order to counteract the zonal momentum sink of the shallow-water thus
235 to conserve AM in the layer over the advective sub-step. The application of this solid-body
236 rotation increment at each dynamical sub-step and for each layer independently is what we call
237 the “level” fixer. The details of the computation are given in Appendix C.

238 Irrespective of whether they are actually applied, the fixer’s velocity increments, Eq.(A13),
239 are vertically interpolated and accumulated over the entire dynamic time-step, and written out
240 diagnostically. In addition to the fixer, partial wind and pressure tendencies arising from the
241 dynamical core are separately diagnosed and written to the standard output streams, providing
242 additional diagnostic tools for cross-checking.

243 Finally, a variant of the fixer was tested in CAM simulations. This variant is a “global”
244 fixer, which still acts by applying an increment to the zonal wind at each sub-step. In this fixer,
245 the apparent torque and the moment of inertia are integrated over all levels within the domain
246 over which strict overall angular momentum conservation is desired. The zonal wind increments
247 then applied as a single solid-body rotational acceleration within this domain. Experimentation
248 showed that such acceleration should not be applied in the stratosphere, where conservation
249 errors are small and the impact of unphysical zonal accelerations large. The necessary limitation
250 of the domain for the global fixer however introduces a certain degree of arbitrariness in its
251 application. Although sometimes used for diagnostic purposes, we do not discuss this fixer
252 variant any further.



253 3 Numerical Simulations and Results

254 3.1 Dry baroclinic wave tests

255 Initial tests were carried out for adiabatic dynamics and flat bottom topography, from baro-
256 clinically unstable initial conditions as defined in Jablonowsky and Williamson (2006; “JW06”).
257 Figure 3 shows the result in terms of conservation of global AM for CAM-FV integrations at
258 f19 resolution (1.9×2.5 degree of latitude and longitude) and 30 hybrid levels.

259 It may be seen that both the correction and the fixer are effective in reducing the systematic
260 numerical sink of AM in these integrations. In particular, the fixer appears to remove it almost
261 completely; in other words, the integration with the fixer conserves global AM in the time
262 mean. This result is central to this paper, and it proves its two main conclusions. The first is
263 that the systematic non-conservation of global AM in the FV dynamical core indeed resides in
264 the advective wind increments of the shallow-water part of the dynamical core. The second is
265 that, by virtue of its effectiveness, and its formulation that is entirely independent of the model
266 configuration or parametrisations (topography, physical momentum sources, etc), the fixer is a
267 useful and accurate general diagnostic tool that allows us to quantify the numerical torque in any
268 CAM-FV integration. By virtue of this quality, the diagnosed time-averaged fixer tendencies
269 were for example used for the perturbations in the experiments shown in Figures 2 and S2.

270 The impact of the correction on conservation is generally smaller, and different dynamical
271 regimes may be seen when the size and quality of that impact changes. In the baroclinic
272 instability tests of Figure 3, the correction achieves good results in the linear and non-linear
273 stages of baroclinic growth (up to day 30; cf JW06), but is not able to correct the slow drift that
274 sets in after zonalisation of the global flow, then wind speed decreases everywhere as a result of
275 numerical dissipation (there are no external sources or sinks of either momentum or energy in
276 these adiabatic simulations). This is a partly desirable behaviour, as the action of the correction
277 should not change the dissipation properties of the scheme.

278 Aside from the conservation properties they are designed for, both the correction and the
279 fixer represent a perturbation of the numerical solutions of the FV dynamical core. By arbi-
280 trarily modifying the relative vorticity associated with the zonal wind, both destroy one of the
281 fundamental numerical properties of the LR97 formulation, viz. the conservation of absolute
282 vorticity under advection. (In the case of the fixer, the vorticity input has a rigid dependency
283 on latitude, $\sin\varphi$). Figure 4a shows their impact on the accuracy of the JW06 baroclinic wave
284 test in terms of root-mean-square (RMS) of the differences in surface pressure from a nominal

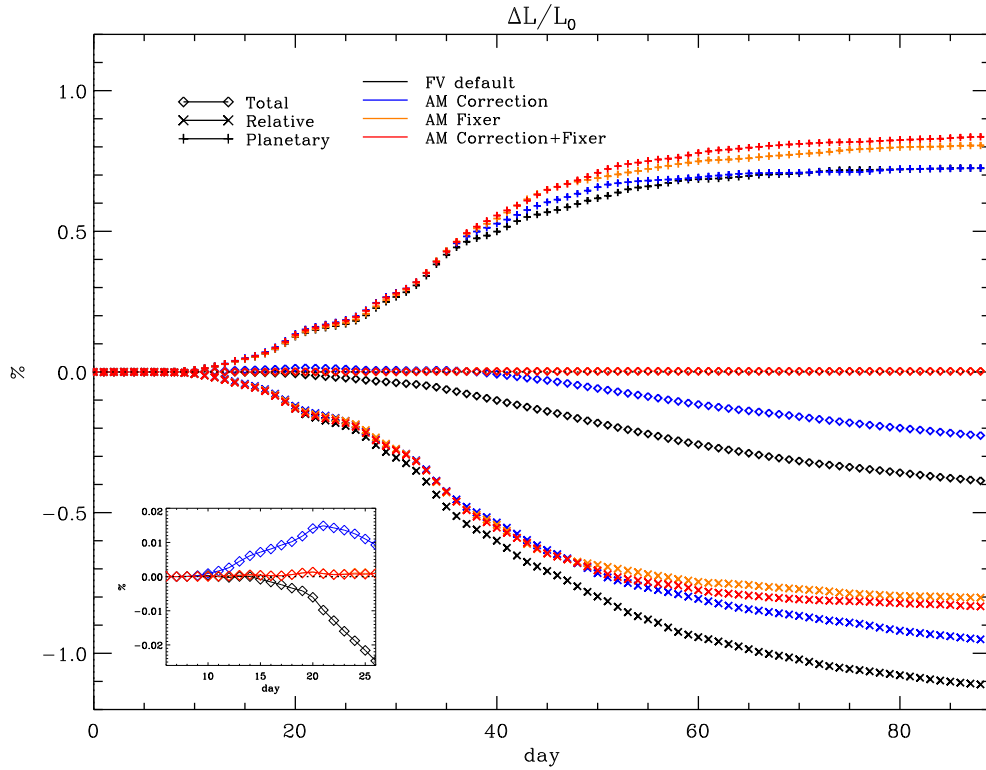


Figure 3: AM correction and fixer in adiabatic, frictionless baroclinic wave tests. Three sets of curves are shown for each of four different simulations with CAM FV, indicating the time evolution of global AM (diamond shapes) and its two components of planetary AM (vertical crosses) and relative AM (x-crosses) in each simulation. Total AM and each AM component are normalised to the initial total AM of the initial state, and differences with respect to initial values are shown, expressed in percentage. Standard CAM-FV is shown in black, CAM-FV with the AM correction only in blue, CAM-FV with the AM fixer only in yellow, and CAM-FV with both AM correction and fixer in red. The inset panel on the lower right of the Figure shows an enlargement for the initial evolution of total AM. Note that the four simulations are nearly indistinguishable before day 8, i.e. during the linear phase of the baroclinic wave. All simulations are run on the two-degree grid.

285 reference solution with original FV dynamical core. The latter is obtained for a resolution of
 286 $0.9^\circ \times 1.25^\circ$, which is sufficiently close JW06's reference solution (cf JW06, Section 5(e), points
 287 (i) and (ii)) for our purposes. It may be seen that on this measure the solutions with and
 288 without the AM corrections are virtually indistinguishable during the stages of both linear and
 289 non-linear baroclinic growth. A similar result holds for the phase (not shown).

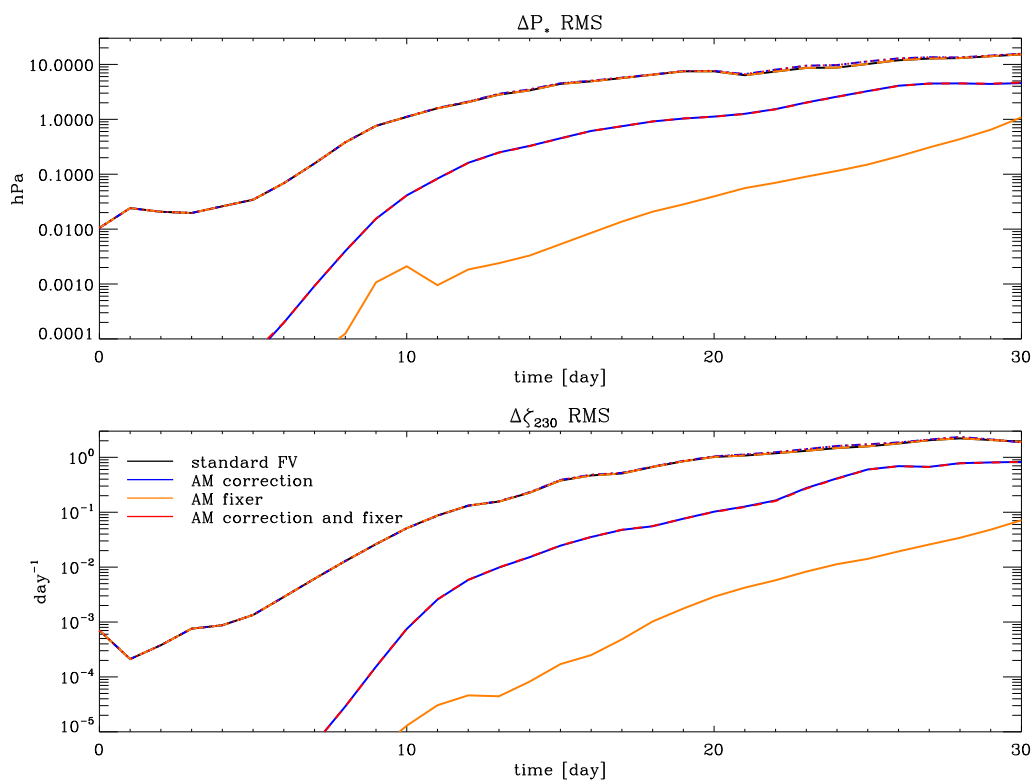


Figure 4: AM correction and fixer in adiabatic, frictionless baroclinic wave test. The simulations shown in Figure 3 are compared with a standard CAM-FV simulation at one degree resolution, and against each other. Each panel shows seven curves, four of which nearly overlap and form the top-most set of lines (including the reference simulation with standard FV). These represent the time evolution of the RMS difference of surface pressure (top panel) and relative vorticity at 230hPa (bottom panel) of each of the two-degree integrations and the control one-degree integration. Below that set of curves are two nearly overlapping curves, which show the RMS differences of the two-degree experiments with AM correction only and the control two-degree integration (blue lines), and of the experiment with both AM correction and fixer and the control integration (red lines). Finally, the single yellow lines at the bottom in each panel show the RMS differences of the two-degree integration with AM fixer only with the two-degree control integration.

290 It may be noted that the largest impact on the RMS of surface pressure arises from the
291 correction. Within the first 30 days this impact is formally always well below significance (as
292 defined in JW06, cf their Figure 10), but it increases in time and eventually becomes appreciable
293 as a full global meridional circulation is established. Similar results hold for the vorticity field,



294 as seen in Figure 4*b*).

295 Other aspects of the solution besides RMS differences also show limited sensitivity to the
296 application of the correction and the fixer. Figure 5 shows the evolution of the minimum pressure
297 in the developing baroclinic wave. By this measure, the solutions only start to diverge with the
298 filling of the primary cyclone and the deepening of the secondary wave after day 17. The solution
299 with the fixer deepens the secondary cyclone more quickly so that the minimum pressure is seen
300 to jump from first to the second wave minimum between days 18 and 19; this occurs one day
301 later with the unmodified dynamical core. A third transition after day 25 has higher central
302 pressure in the solutions with the fixer; by this time, however, rapid cyclogenesis is occurring
303 in the jet stream of the southern hemisphere, attaining a similar minimum pressure, which is
304 slightly deeper in the solutions with the fixer. In any case the pressure differences of the minima
305 remain of the order of a few hPa, and there is no systematic difference in their position.

306 **3.2 Other idealised tests**

307 Even if the impacts of the modifications of the FV dynamical core are relatively small on local
308 circulations over subseasonal time-scales, as shown above, the rationale for introducing them is
309 the hope of achieving a better simulation of the state of the atmosphere in integrations under
310 specified forcings. As explained in the introduction, one particular expectation is that the
311 subtropical easterlies should weaken, without affecting the circulation elsewhere too heavily. In
312 particular the role of the correction, which alone does not ensure AM conservation, must be
313 clarified, and its eventual use justified. Here we document the results of two sets of idealised
314 simulations that still have a simplified, equipotential lower boundary, but include non-vanishing
315 physical torques and heating tendencies.

316 The first set of such simulations adhere to the benchmark test of Held and Suarez (1994; “HS”
317 henceforth), where the forcing has the form of a relaxation towards a specified three-dimensional
318 atmospheric temperature field. Likewise, surface friction is represented by a damping of the
319 winds within a set of levels near the bottom boundary. Apart from the small numerical diffu-
320 sion, these stresses are communicated to the rest of the atmosphere only by means of momentum
321 advection in the global circulation. The second set of simulations follows the Aquaplanet (“AP”)
322 test first proposed by Neale and Hoskins (2000), where only a persistent field of bottom-boundary
323 temperatures is prescribed (the “QOBS” profile of Neale and Hoskins 2000), and the full set of
324 moist atmospheric physical parametrisations of CAM6 are used to force the circulation (except

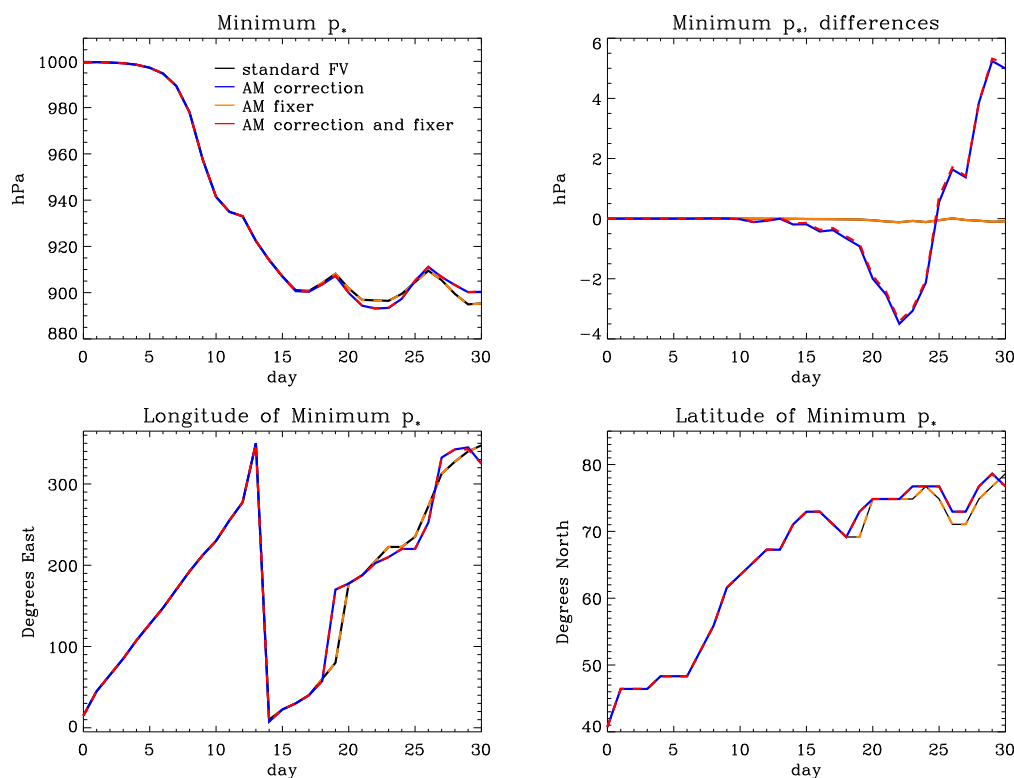


Figure 5: AM correction and fixer in adiabatic, frictionless baroclinic wave test. Evolution of minimum pressure (panel on the top-left) and its position (panels at the bottom) in the baroclinic-wave evolution from the integrations shown in Figure 3. Colour-coding of the lines is the same as in Figure 3. The panel on the top-right show the differences in minimum pressure between the AM experiments and FV control, with the same colour coding as in the lower curves in Figure 4.

325 for those specific to orographic processes). The bottom boundary is a notional static ocean with
326 unlimited heat and water capacity. Surface stresses are computed by the coupler, and passed
327 to the moist atmospheric boundary-layer parametrisation which then distributes those stresses
328 vertically. Momentum is also transported in moist convection, where active, and further adjust-
329 ments are made when the moist mass of the atmospheric column changes due to precipitation
330 and surface evaporation processes. To simplify the analysis, the gravity-wave parametrisation
331 of CAM6 was turned off in our AP tests. In both sets of tests, FV's advection scheme is used
332 at PPM's standard fourth-order at all levels, i.e. the numerical diffusion obtained in standard



333 CAM-FV integrations by employing low-order calculations near the model top is avoided. For
 334 initial conditions, HS simulations are cold-started with uniform surface pressure and geopo-
 335 tential, and vanishing wind fields except for a westerly perturbation identical to that used in
 336 the dry baroclinic wave tests (necessary in order to break zonal symmetry and to allow a non-
 337 vanishing correction). The AP simulations all take the same instantaneous atmospheric state
 338 from a previous spun-up run, even though this requires more adjustment for the corrected/fixed
 339 simulations than for the control.

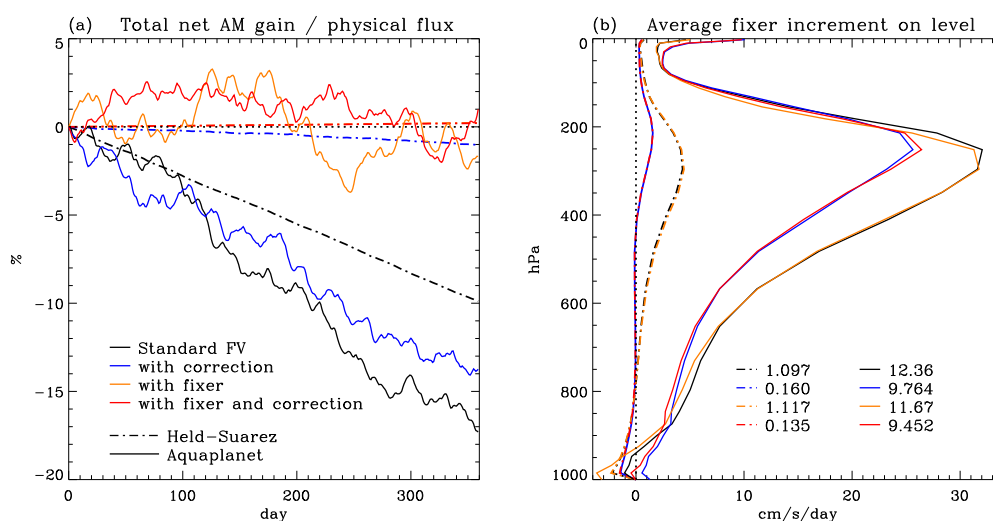


Figure 6: AM correction and fixer in Held-Suarez (HS) and Aquaplanet (AP) integrations. Panel (a) shows the time evolution of total AM for each of the integrations, similar to Figure 3 (diamond shapes) but normalised, separately for each integration, to the time-integrated physical (i.e. surface stress) torque at day 360. AP integrations are shown in solid, HS integrations in stippled lines. The colour coding is as in Figure 3. Panel (b) shows the time-mean numerical torque, averaged over days 120-360, arising at each model level from advective increments, as diagnosed by the fixer, and expressed as equatorial acceleration in a solid-body rotation required to compensate for the numerical sink. Line types and colours correspond to those shown in panel (a). The lists at the bottom of panel (b) indicate the time-mean equatorial accelerations of a *global* solid-body rotation, i.e. the increments shown by the lines but integrated vertically level by level, weighted with the appropriate moments of inertia.

340 Figure 6a indicates that the global AM conservation properties of the simulations in these
 341 tests are broadly in line with the expectations from the previous discussion. Standard FV tests
 342 (black lines) show a steady loss of AM in the atmospheric circulation, of a magnitude of the order
 343 of 10-20% of the physical flux of momentum through the atmosphere. (We count eastward stress



344 as positive, by which the atmosphere gains westerly momentum in the tropical surface easterlies,
345 and loses westerly momentum in the subtropical surface westerlies). Use of the correction leads
346 to an order-of-magnitude reduction of the numerical sink of AM in HS integrations, but it is
347 of limited effectiveness in full-physics AP integrations (blue lines). Integrations with the fixer,
348 with or without the correction (orange and red lines, respectively), maintain atmospheric AM
349 in the time mean. In HS simulations, there appears to be a very small residual drift of AM
350 notwithstanding the fixer. This is due to a small inconsistency in the application of the stress
351 terms, which are calculated and diagnosed in the “physics” part of the model time-stepping,
352 but applied later as velocity tendencies in the physics-dynamics interface on updated layer
353 masses. This is an intrinsic feature of the time-stepping of CAM-FV that we have not modified.
354 More notably, AP simulations differ from HS simulations in that they show obvious fluctuations
355 of total AM around the time mean or around the long-term drift, when there is one. Such
356 fluctuations are similar in all AP integrations, with a magnitude of a few percent of the physical
357 sources, and depend on non-conservation in CAM’s physics parametrisations. Fortunately, they
358 are not systematic and do not produce a noticeable long-term drift.

359 The effectiveness of the fixer in removing most of the AM drift confirms that the systematic
360 sink of AM in CAM-FV integrations arises predominantly from the shallow-water advection
361 calculations. The accuracy of the correction, by contrast, depends on the features of the cir-
362 culation, with good accuracy for numerical well-resolved features, as in the HS tests, but a
363 poorer one when grid-scale forcing associated with the water cycle occurs. Figure 6b gives more
364 details on the effect of the correction. Here, the time-average AM sink due to the dynamical
365 core is diagnosed using the fixer increments for the zonal velocity at the equator at each model
366 level. This diagnostic is produced irrespective of whether such increments are applied during
367 the integration. Apart from the smaller increments in HS integrations than in AP integrations,
368 which partly depend on the slower circulation (“surface” stresses are one order of magnitude
369 larger in the HS set-up than in the AP set-up), the advective AM sink has a distinctive shape in
370 pressure-level space, with a maximum in the upper troposphere and small values in the atmo-
371 spheric boundary layer. This shape partly reflects the underlying global-mean zonal wind field,
372 but the maximum sink lies below the maximum wind (at around 250 hPa rather than around
373 150 hPa). The profile of the impact of the correction, i.e. the reduction in fixer increments
374 when the correction is applied, has again a similar shape but with an even lower position of the
375 maximum, which better corresponds with the maximum in the vertical profile of level-integral
376 zonal momentum of the underlying flow. Combined with the off-line diagnostic information for



377 the apparent AM sink from Figure 1, it can be deduced that the main loci of the time-mean
378 AM sink in these simulations are found near the subtropical jet streams, where large zonal
379 asymmetries occur in both the mass fields and the wind fields.

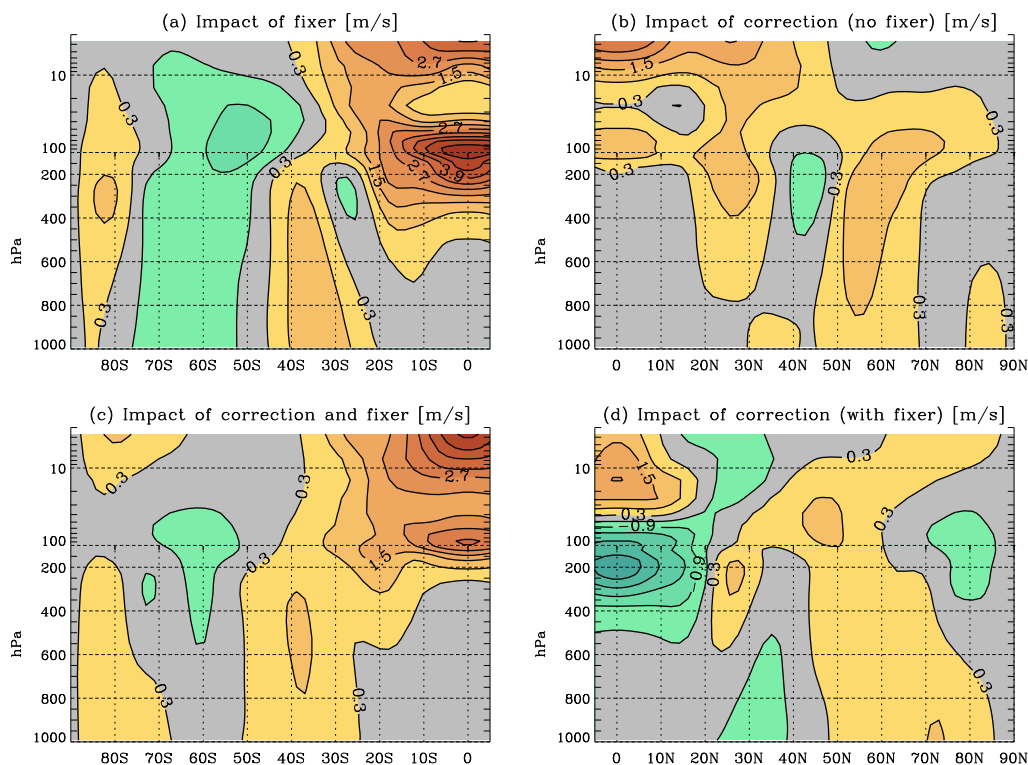


Figure 7: Impact of AM correction and fixer in Held-Suarez simulations. Time-mean vertical latitude-pressure profiles of wind differences between HS simulations shown in the stippled lines in Figure 6. Panel (a) shows the zonal-mean zonal-wind time-average (days 120-360) difference field of the integration with AM fixer only and the control integration. Panel (b) shows the same field, but for the difference between the integration with AM correction and control. Panel (c) shows the difference between the integration with both AM correction and AM fixer and control, and panel (d) that between the integration with both AM correction and AM fixer and the integration with AM fixer only. The contour interval is 0.6 m/s, with blue hues indicating negative values, and red hues positive values. Values in the interval $[-0.3,+0.3]$ m/s are left in grey.

380 The effect on the mean circulation of applying the correction and/or the fixer are shown in
381 Figures 7 and 8 for HS and AP simulations, respectively. The zonal-mean zonal winds are shown,

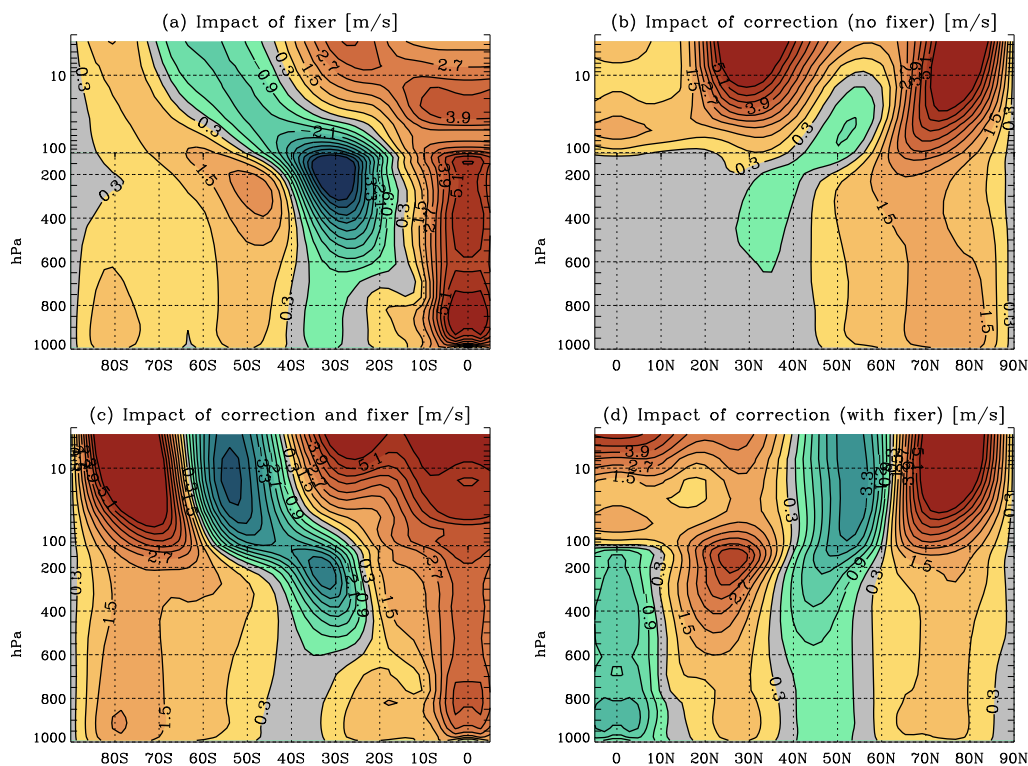


Figure 8: Impact of AM correction and fixer in Aquaplanet simulations. Same as Figure 7, but for the AP simulations shown in the solid lines in Figure 6.

382 which is the quantity that both the correction and the fixer directly modify. Nevertheless, it
383 should be remembered that the net effect is indirect, since the zonal winds remain in the time-
384 average close to geostrophic balance with the (equivalent) temperature field. In HS simulations,
385 the local temperature differences between simulations are simply proportional to the difference
386 in temperature advection by the meridional and vertical circulation, which is modified primarily
387 through a “tea leaves” mechanism. As already seen in the Introduction, the leading-order effect
388 of the fixer is a weakening of this circulation, and thus of the associated advective temperature
389 tendencies. These tend to cool the lower troposphere in the subtropical easterlies, cool the upper
390 troposphere near the equator, and warm the troposphere poleward of the jet streams. The effect
391 of the fixer on the zonal-mean zonal wind shown in Figure 7a is generally consistent with this
392 expectation, with an equatorward retreat of the surface easterlies and weaker westerlies in the



393 higher latitudes. There is, however, an additional large westerly difference near the equatorial
394 tropopause, which is a direct consequence of the westerly forcing of the fixer, which is greatest
395 at the Equator. This is clearly an undesirable effect of the fixer on the simulations. A more
396 selective effect on the circulation is produced by the correction (Figure 7b). As seen above, its
397 main action is in where the greatest sink of AM is located, i.e. on the flanks of the subtropical
398 jet stream. By correcting part of the AM non-conservation, it also acts to limit the action of
399 the fixer (Figure 7d). As a result, the combination of correction and fixer together, as well
400 as ensuring good global AM conservation, is less severe in terms of its upper-level equatorial
401 westerly effect (Figure 7d). This suggests that the fixer is best employed in combination with
402 the correction.

403 In AP simulations, a slow-down of the meridional circulation is still expected and found,
404 but the interaction between dynamical forcing by the fixer or the correction and the physics
405 tendencies is much more complex and difficult to predict. The fixer now produces large westerly
406 differences near the equator at all levels, and a marked weakening of the subtropical jet stream
407 (Figure 8a). The equatorial winds above 300hPa become westerly. The correction is less effective
408 overall than in HS simulations, and its impacts are mostly confined to level close to the model
409 lid or to the high latitudes (Figure 8b). Nonetheless, its use is still beneficial in terms of limiting
410 the action of the fixer, at least in the troposphere (Figure 8d). The result of the combined
411 correction and fixer can be seen in Figure 8c. In terms of tropospheric impacts, it appears
412 acceptable; equatorial winds remain easterly below 200hPa, and weak above. The weakening
413 of the equatorial and tropical easterlies compared with the control simulation implies greater
414 similarity with simulations with AM-conserving spectral models. Large changes however can
415 be seen near the model lid, especially in the four model layers with pressures less than 25
416 hPa. This is a consequence of momentum accumulation within these layers. In CAM's default
417 configuration, the order of FV's PPM advection scheme is reduced here, which results in large
418 numerical dissipation. Effectively, these levels are used as sponge layers and are thus not part of
419 the valid computational domain of the model. In full-model configurations it is therefore advised
420 to keep the reduced order of advection and turn off both the correction and the fixer in these
421 layers. The large mean-state changes seen near the top in Figure 8d then vanish. Considering
422 the troposphere only, the conclusion obtained from HS simulations can be seen to hold also
423 for full-physics AP model simulations, in that the combined application of the fixer and the
424 correction results in smaller overall mean-state changes of the solution compared to default FV
425 without modifications, while ensuring good conservation of AM.

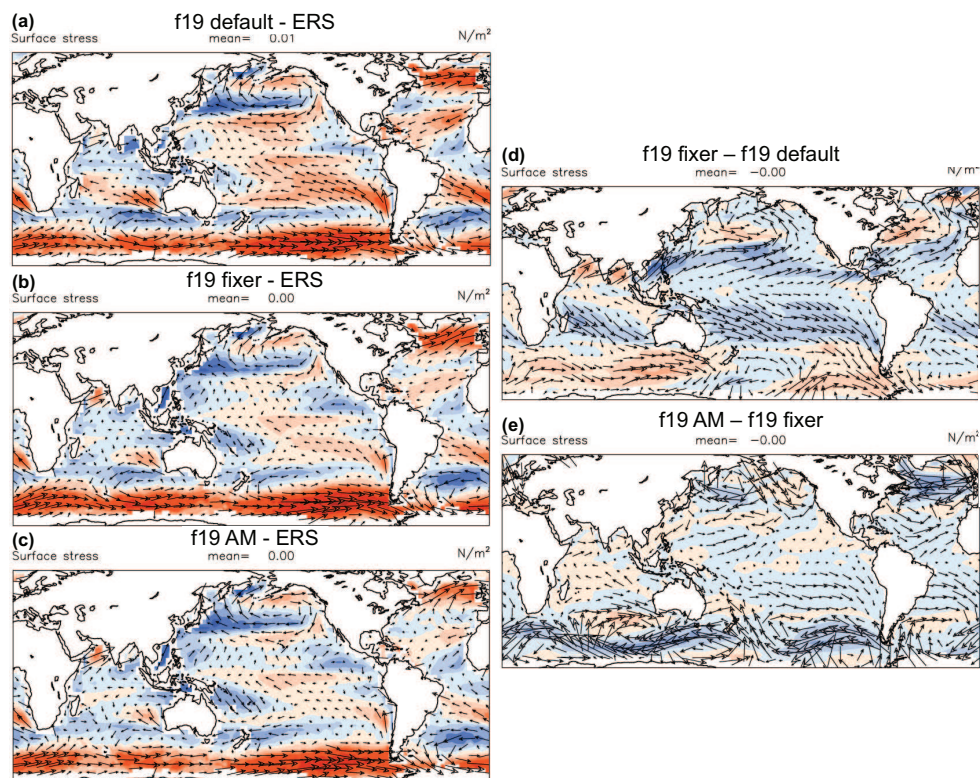


Figure 9: Impact of AM correction and fixer in F2000 simulations. Panels (a), (b) and (c) show maps of surface wind-stress vector differences (arrows) and wind-stress magnitude differences (colours) between “F2000” simulations with CAM-FV at $1.9^{\circ} \times 2.5^{\circ}$ degree resolution (“f19”) and a climatology obtained from satellite scatterometer observations (ERS; Quilfen et al. 1999). Panel (a) shows the annual-mean climatological bias in the f19 control integration; panel (b) for a f19 simulation with AM fixer only; and panel (c) for an f19 simulations with both AM correction and AM fixer. Panels (d) and (e) show the same fields, but for the differences between the simulation with fixer only and control, and between the simulation with both fixer and correction and that with fixer only. The colour scale for all plots is on the right of panels (d) and (e). These plots were produced with the AMWG diagnostics package developed by the Atmospheric Model Working Group of the University Corporation for Atmospheric Research and the National Center for Atmospheric Research.

426 4 Simulations of the observed climatology

427 The relevance of the AM modifications to the FV dynamical core for CAM simulations in realistic
428 configuration is investigated here using “F2000” cases, where SSTs and all compositional forcings



429 are prescribed as a repeating annual cycle obtained from an observed climatology of the decade
430 spanning the turn of the century. We test at two grid resolutions, one of $1.9^{\circ} \times 2.5^{\circ}$ (“f19”) as in
431 all integrations already discussed above, and one of $0.9^{\circ} \times 1.25^{\circ}$ (“f09”), to test the impacts of
432 AM modifications in a case that is scientifically supported by NCAR at this time. The CESM
433 model version used (here as above) is release 2.1.1¹

434 Figure 9 illustrates the effects of the fixer and the correction on f19 simulations. The control
435 simulation shows a characteristic easterly surface wind-stress bias throughout the Tropics (Figure
436 9a). In addition, there are excessive westerlies at southern high latitudes. The effect of the fixer
437 is to reduce the tropical biases (Figure 9b), with an evident westerly effect on the simulations
438 nearly symmetrically about the equator (Figure 9d). By that same token, however, the high-
439 latitude westerly errors are enhanced (Figure 9b). The application of the correction in addition
440 to the fixer not only brings further improvements in the tropics, but also corrects the westerly
441 effect of the fixer in high latitudes (Figure 9e). The result is a significant improvement in the
442 simulation of the surface wind-stress field over the entire ocean domain.

443 In general, we obtain a similar conclusions as for the AP simulations. The impact of the
444 correction on the global conservation of AM is modest, removing only about 15% of the sink at
445 f19 resolution. However, its action is stronger on upper-level winds (cf. Figure 6b), which leads
446 to proportionally reduced fixer increments at those levels, and thus to smaller impacts by the
447 fixer on areas affected by baroclinic instability.

448 Figure 10 and Figure S3 in the supplementary information shows the seasonally resolved
449 impacts on the zonal-mean zonal winds from applying the combination of fixer and correction
450 in F2000 simulations at both f19 and f09 resolutions (cf also Figure S3 in the supplementary
451 information, for JJA). In all cases, the reduction of biases in both easterly and westerly wind
452 regimes is noticeable, the latter especially at the sub-polar latitudes of the winter hemisphere.

453 More in detail, it may be noted that the benefits of the AM modifications appear more
454 clearly for the winds in the simulation at the lower resolution, where the numerical sink of AM
455 is indeed larger. These benefits however are not limited to the zonal-mean zonal winds, and
456 they are also appreciable at the f09 resolution. Most notable is the reduction in the strength
457 of the Hadley circulations (cf Figure S4 in the Supplementary Information), which is expected
458 from the arguments set out in the Introduction. This has consequences for many aspects of the

¹More precisely, we used a pre-release of CESM2.1.1 (#20, 22 March 2019). In terms of the simulations presented in this paper, the differences with the full 2.1.1 release only affect the F2000 cases at f19 resolution, where slightly different emission datasets are used to force the simulations. The impacts of this are of negligible consequence for the results discussed in this Section.

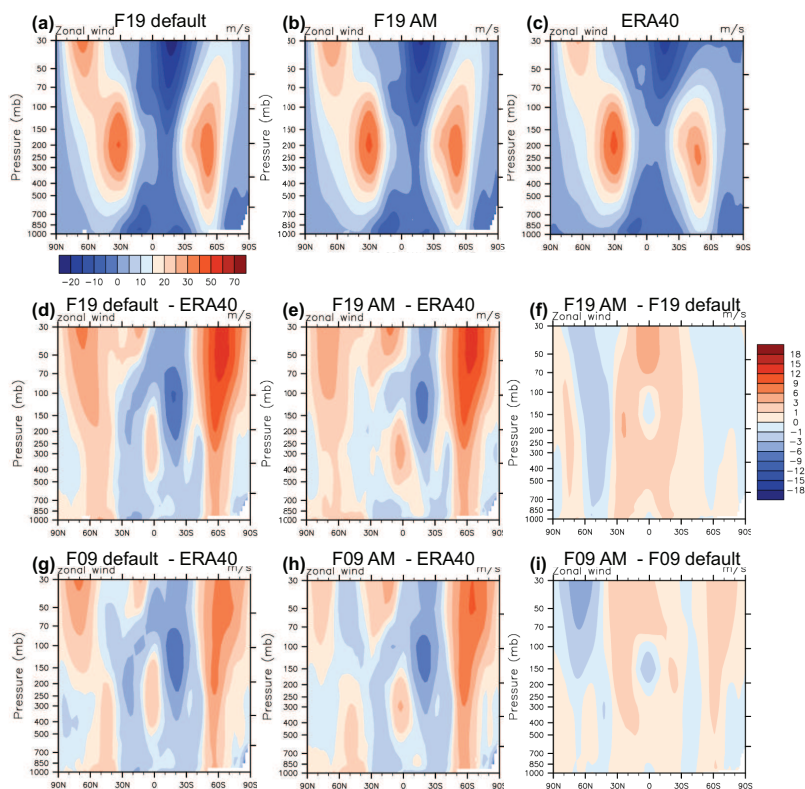


Figure 10: Impact of AM correction and fixer in F2000 simulations. Latitude-pressure maps of zonal-mean zonal wind climatologies for boreal winter (DJF). Panels (a), (b) and (c) show total fields for the CAM-FV f19 control simulation, (panel (a)) for the f19 simulation with both AM fixer and AM correction (panel (b)), and for the ERA40 reanalysis (Uppala et al., 2005). The colour scale is at the bottom of panel (a). Panels (d) and (e) show the differences of each of the two f19 integrations and ERA40, and panel (f) shows the differences between the two f19 simulations. The colour scale is on the right of Panel (f). Panels (g), (h), and (i) are analogous to panels (d), (e), and (f), respectively, but for CAM-FV simulations at $0.9^{\circ} \times 1.25^{\circ}$ resolution. These plots were produced with the AMWG diagnostics package developed by the Atmospheric Model Working Group of the University Corporation for Atmospheric Research and the National Center for Atmospheric Research.

459 global circulation. Figure 11 shows a summary of the impacts on the quality of the simulations
 460 in relation to the observed climatology. The improvements at f09 seems particularly remarkable
 461 considering that the unmodified simulation is a scientifically supported case that has been fully
 462 tuned for a best match to observations. It may be noted that no additionally tuning whatsoever

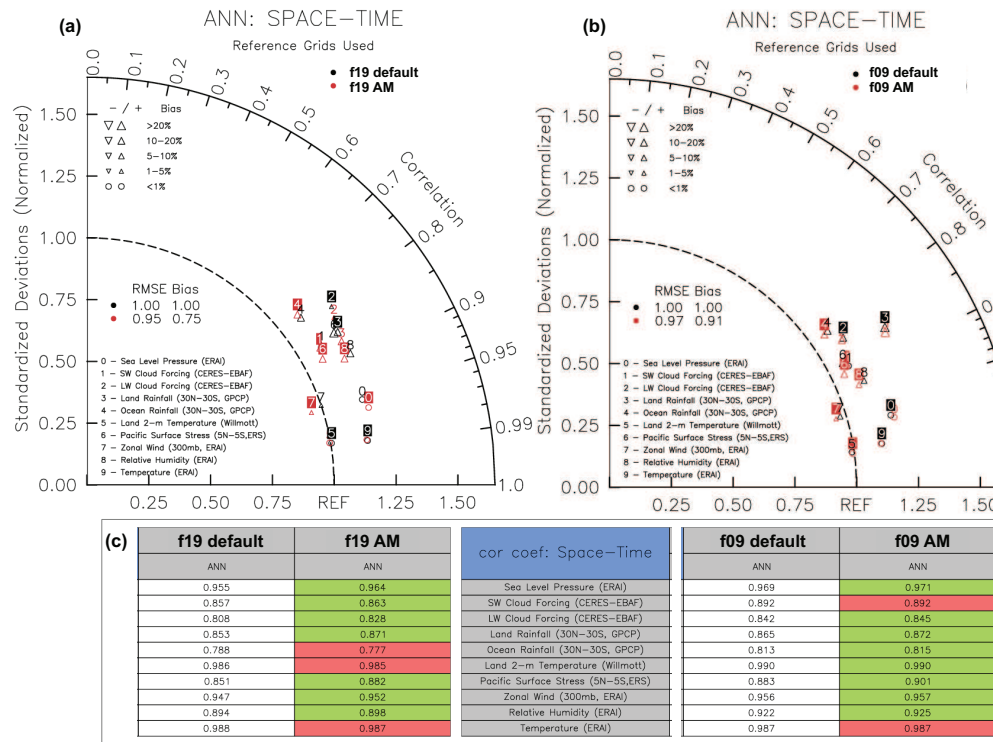


Figure 11: Impact of AM correction and fixer in F2000 simulations. Panels (a) and (b) show Taylor (2001) diagrams for the validation of the CAM-FV “F2000” simulations at f19 (panel (a)) and at f09 (panel (b)) resolution against observations for a standard set of diagnostic fields, listed in the panels. Black symbols represent RMS differences to observations for the control simulations without modifications, and red symbols for the simulations using both the AM correction and the AM fixer. For the overall RMSE and bias scores, those from the control simulations are used as normalisation. Panel (c) summarises the correlation values between simulated and observed diagnostic fields as listed in the central table. Green fields mark all instances where one of the AM-modified simulation represents an improvement over the respective control simulation. These plots were produced with the AMWG diagnostics package developed by the Atmospheric Model Working Group of the University Corporation for Atmospheric Research and the National Center for Atmospheric Research.

463 is involved in the simulation with AM modifications shown here, and that the AM modifications
 464 themselves have no free parameters as they follow directly from an effort to reduce the numerical
 465 sink stemming from the FV dynamical core. The better quality of this simulation thus follows



Table 1: Simulation set-ups and the effect of AM modifications

Simulations (FV19, 2°)		A	B	C
experiment	description	HS dt=225s	AP dt=225s	F2000 dt=225s
1	geometry and pressure only ¹	-7.1%	-23.8%	-26.5%
2	AM correction ²	0.3%	-19.8%	-24.7%
3	2 + AM fixer ³	0.7%	1.9%	0.8%

¹Sections 2.2 and 2.1

²Section 2.3

³Section 2.3 and Section 2.4

466 entirely from better adherence of the solution to a fundamental property of the equations of
467 motion.

468 5 Summary and Conclusions

469 AM conservation in CAM-FV has been substantially improved by means of a correction that
470 reduces the zonal-mean numerical sink of Lin and Rood's (1997) shallow-water scheme, and a
471 fixer that ensures conservation of global angular momentum under advection. The effective-
472 ness of these modification in terms of AM conservation in the simulations presented here is
473 summarised in Table 1. We show that aside from global AM conservation, they have other sig-
474 nificant impacts on the simulations, consistent with the "tea-leaves" mechanism (Einstein 1926)
475 that rapidly redistributes pressure forces in a rotating fluid in response to zonal accelerations.
476 The most notable effect is a reduction of the excessive easterlies of the model, with a concomi-
477 tant slow-down of the Hadley circulation. As a result of such changes, the simulations of the
478 observed climatology shows marked improvements.

479 The zonal-mean correction of the shallow-water scheme is not necessary for enforcing global
480 conservation, as this can be achieved by the fixer alone. Indeed, the correction is quite ineffective
481 in realistic simulations of the atmosphere in terms of global conservation. Nevertheless, we
482 find that its concomitant application with the fixer has positive impacts on the simulations.
483 In particular, it reduces the effects of the fixer in the mid-latitudes. This can be explained



484 with the greater effectiveness of the correction in the baroclinically unstable regions around the
485 subtropical jet streams, where local the (zonal-mean) numerical sink appears to be largest. Even
486 so, because of its potentially large local effects, the utilisation of the correction under different
487 set-ups should be tested on a case-by-case basis according to its impacts on the results.

488 Improving the quality of the simulation of the global distribution of surface wind-stress should
489 be expected to bring particular benefits to coupled atmosphere-ocean simulations. An adequate
490 discussion of such coupled simulation would exceed the scope of the present manuscript, which is
491 aimed primarily at presenting the method. In particular, due to their computational expense, at
492 the present time it is not possible to produce well spun-up coupled simulations that can provide
493 an assessment of the impact of the AM modifications.

494 The modification to the FV dynamical core that we describe and utilise are relatively crude,
495 and cause local loss of accuracy due to violation of vorticity conservation under advection.
496 Nevertheless, the associated detrimental impacts appear to be fairly limited, with insignificant
497 differences under standard tests such as the Jablonowsky and Williamson (2006) baroclinic wave
498 test, which should be sensitive to local conservation. Even so, it is clear from the very same tests
499 that simulations over weather time-scales are not sensitive to AM conservation, so that for such
500 application it is not advisable to trade enforcing such conservation for a loss of accuracy. On the
501 longer time-scales of climate simulations, by contrast, our results demonstrate the importance
502 of global conservation of atmospheric AM in order to obtain a realistic global circulation.



503 **Code and data availability.**

504 The code used in the numerical simulations of this paper is available under

505 <https://zenodo.org/badge/latestdoi/214872045>

506 CAM6 is published in the open-access CESM ESCOMP git repository, freely available under
507 <https://github.com/ESCOMP>. The AM options can be switched on by setting standard CAM
508 namelist parameters to non-default values (i.e. T instead of F; there are no free numerical
509 parameters). Apart from these switches, all atmosphere model configurations presented in this
510 paper are standard CESM cases that can be set up and run using the scripts provided in the
511 repository. Users can obtain technical support if requested.

512 **Author Contributions:** Thomas Toniazco conceived the idea, proposed the work, made the
513 calculations, implemented the code, ran the simulations, evaluated them, produced all figures,
514 and wrote the manuscript. Mats Bentsen supported this activity through national infrastructure
515 projects of the Norwegian Research Council. Cheryl Craig, Brian Eaton and James Edwards
516 revised the code and included it in the official ESCOMP CESM repository. Steven Goldhaber
517 gave technical advice on CAM code and simulations. Peter Lauritzen, Mats Bentsen, and
518 Christiane Jablonowski were at hand for critical discussion of the scientific ideas and helped
519 providing the initial impetus of this work. Mats Bentsen, James Edwards, Steve Goldhaber,
520 and Peter Lauritzen also provided useful comment and suggestions on the draft manuscript.

521 **Acknowledgements:** Warm thanks go to Prof. Christoph Heinze for his unbending dedi-
522 cation to model development in the NorESM consortium and allowing in particulat this work to
523 go forward. We are grateful to Dr. Alok Gupta at NORCE and Dr. Cecile Hannay at NCAR
524 for their crucial work in carrying out and supporting NorESM and CESM development simu-
525 lations. This work was partially funded by Norwegian Research Council grant #229771 (EVA)
526 and #270061 (INES).



527

References

528

Arakawa, A., and V.R. Lamb, 1981: A potential enstrophy and energy conserving scheme for the shallow water equations. *Mon. Wea. Rev.* 109, 18-36.

529

530

Blackburn, M., D. L. Williamson, K. Nakajima, W. Ohfuchi, Y. O. Takahashi, Y.-Y. Hayashi, H. Nakamura, M. Ishiwatari, J. L. McGregor, H. Borth, V. Wirth, H. Frank, P. Bechtold, N. P. Wedi, H. Tomita, M. Satoh, M. Zhao, I. M. Held, M. J. Suarez, M.-I. Lee, M. Watanabe, M. Kimoto, Y. Liu, Z. Wang, A. Molod, K. Rajendran, A. Kitoh, and R. Stratton: The Aqua-Planet Experiment (APE): CONTROL SST simulation. *J. Meteor. Soc. Japan*, 91A, 17-56, doi:10.2151/jmsj.2013-A02. 2013.

531

532

533

534

535

536

Colella, P., and P.R. Woodward: The piecewise parabolic method (PPM) for gas-dynamical simulations. *J Comp Phys* 54 , 174-201. 1984.

537

538

Egger, J., and K.-P. Hoinka: The annual cycle of the axial angular momentum of the atmosphere. *J. Climate* 18, 757-771. 2005.

539

540

Einstein, A.: Die Ursache der Mäanderbildung der Flußläufe und des sogenannten Baer-schen Gesetzes. *Die Naturwissenschaften* 11, 223-224. 1926.

541

542

Feldl, N. and S. Bordoni: Characterizing the Hadley circulation response through regional climate feedbacks. *J. Climate*, 29, 613622, doi:10.1175/JCLI-D-15-0424.1. 2016.

543

544

Hadley, G.: Concerning the cause of the general trade-winds. *Phil. Trans.* 39, 58-62. 1735.

545

546

Held, I.M., and A.Y. Hou: Nonlinear axially symmetric circulations in a nearly inviscid atmosphere. *J. Atmos. Sci.* 37, 515-533. 1980.

547

548

Held, I. M., and M. J. Suarez: A proposal for the intercomparison of the dynamical cores of atmospheric general circulation models, *Bull. Am. Meteorol. Soc.*, 75, 1825-1830. 1994.

549

550

Hollingsworth, A., Killberg, P., Renner, V., and D.M. Burridge: An internal symmetric computational instability. *Q. J. R. Meteorol. Soc.* 109 , 417-428. 1983.

551

552

Jablonowski, C., and D. L. Williamson: A Baroclinic Instability Test Case for Atmospheric Model Dynamical Cores, *Quart. J. Roy. Met. Soc.*, Vol. 132, 2943-2975. 2006.

553



- 554 Quilfen, Y., B. Chapron, A. Bentamy, J. Gourrion, T. Elfouhaily, and D. Vandemark:
555 Global ERS-1/2 and NSCAT observations: Upwind/crosswind and upwind/downwind
556 measurements. *J. Geophys. Res.*, 104, 1145911469. 1999.
- 557 Laprise, R., and C. Girard: A spectral general circulation model using a piecewise-constant
558 finite-element representation on a hybrid vertical coordinate system. *J. Climate* 3, 32-52.
559 1990.
- 560 Lauritzen P.H., Bacmeister J.T., Dubos T., Lebonnois S., and M.A. Taylor: Held-Suarez
561 simulations with the community atmosphere model spectral element (CAM-SE) dynamical
562 core: a global axial angular momentum analysis using Eulerian and floating Lagrangean
563 vertical coordinates. *J. Adv. Model. Earth Syst.* 6, 129-140. doi:10.1002/2013MS000268.
564 2014.
- 565 Lebonnois, S., C. Covey, A. Grossman, H. Parish, G. Schubert, R. Walterscheid, P. H.
566 Lauritzen, and C. Jablonowski: Angular momentum budget in general circulation mod-
567 els of superrotating atmospheres: A critical diagnostic, *J. Geophys. Res.*, 117, E12004,
568 doi:10.1029/2012JE004223. 2012
- 569 Lin, S.J.: A finite-volume integration method for computing pressure gradient force in
570 general vertical coordinates. *Quart. J. R. Meteorol. Soc.* 123 , 1749-1762. 1997.
- 571 Lin, S.J., and R.B. Rood: An explicit flux-form semi-Lagrangian shallow-water model on
572 the sphere. *Quart. J. R. Meteorol. Soc.* 123 , 2477-2498. 1997.
- 573 Lin S.-J.: A “vertically lagrangian” finite-volume dynamical core for global models. *Mon.*
574 *Wea. Rev.* 132, 2293-2307. 2004.
- 575 Lindzen, R.S., and A.Y. Hou: Hadley circulations for zonally averaged heating centered
576 off the equator. *J. Atmos. Sci.* 45, 2416-2427. 1988.
- 577 Lipat, B. R., G. Tselioudis, K. M. Grise, and L. M. Polvani: CMIP5 models shortwave
578 cloud radiative response and climate sensitivity linked to the climatological Hadley cell
579 extent, *Geophys. Res. Lett.*, 44, 57395748, doi:10.1002/2017GL073151. 2017
- 580 Neale, R. B., and B. J. Hoskins: A standard test for AGCMs including their physical
581 parameterizations. II: Results for the Met Office model. *Atmos. Sci. Lett.*, 1, 108114,
582 doi:10.1006/asle.2000.0024. 2000.



- 583 Pauluis, O.: Boundary layer dynamics and cross-equatorial Hadley circulation. *J. Atmos.*
584 *Sci.* 61, 1161-1173. 2004.
- 585 Schneider, E.K.: Axially symmetric steady-state models of the basic state for instability
586 and climate studies. Part II: Nonlinear calculations. *J. Atmos. Sci.* 34, 280-297. 1977
- 587 Simmons, A.J., and D.M. Burridge: An energy and angular-momentum conserving vertical
588 finite-difference scheme and hybrid vertical coordinates. *Mon Wea Rev* 109 , 758-766. 1981.
- 589 Taylor, K.E.: Summarizing multiple aspects of model performance in a single diagram. *J.*
590 *Geophys. Res.* 106, 7183-7192. 2001.
- 591 Uppala, S. M., and Coauthors: The ERA-40 Re-Analysis. *Quart. J. Roy. Meteor. Soc.*,
592 131, 29613012. 2005.
- 593 Walker, C.C., and T. Schneider: Eddy influences on Hadley circulations: simulations with
594 an idealized GCM. *J. Atmos. Sci.* 63, 3333-3350. 2006.
- 595 White, A.A., Hoskins, B.J., Roulstone, I., and A. Staniforth: Consistent approximate
596 models of the global atmosphere: shallow, deep, hydrostatic, quasi-hydrostatic, and non-
597 hydrostatic. *Quart. J. Roy. Meteorol. Soc.* 131, 2081-2107. 2005.



598 A Off-line diagnostics of numerical torque in model sim- 599 ulations

600 The diagnosis of the residual torque that violates AM conservation in CAM simulations follows
 601 from the hydrostatic Primitive Equations (cf. White et al. 2005). In our zonally and vertically
 602 integrated diagnostics such as in Figure 1 the AM source is calculated as

$$S_M = \partial_t L_r + D_L - T_x - C_\lambda \quad (\text{A1})$$

603 where the first term on the r.h.s. represent the tendency of relative atmospheric AM, the second
 604 term represent the divergence of AM flux, the third the physical torque (which in all simulations
 605 presented in Sections 1, 2, and 3, when non-vanishing, is exclusively due to surface stresses or
 606 linear friction in the PBL), and the last term is the tendency in absolute atmospheric AM. In
 607 formulas:

$$\begin{aligned} L_r &= \int_0^{2\pi} \int_{p_*}^{p_{top}} (ua \cos \varphi) \frac{dp}{g} a \cos \varphi d\lambda \\ D_L &= \frac{1}{a} \frac{\partial}{\partial \varphi} \int_0^{2\pi} \int_{p_*}^{p_{top}} (uva \cos \varphi) \frac{dp}{g} a \cos \varphi d\lambda \\ T_x &= \int_0^{2\pi} (\tau_x a \cos \varphi) a \cos \varphi d\lambda \\ C_\lambda &= -\frac{a\Omega \sin 2\varphi}{g} \partial_t \int_0^{2\pi} \int_0^\varphi p_* a^2 \cos \varphi' d\varphi' d\lambda, \end{aligned}$$

608 where a is the Earth's radius, φ the latitude, λ the longitude, g the gravitational acceleration in
 609 Earth's surface, Ω the angular speed of Earth's rotation, and u , v , p_* and τ_x are the zonal wind
 610 component, the meridional wind component, the surface pressure, and the zonal component of
 611 the surface or frictional stress acting on the air in the model simulations. Note that to obtain
 612 C_λ the continuity equation was used. Note that for the time-average values of S_M , the time
 613 differentials become increments between the initial and the final state; terms T_x and C_λ are linear
 614 in the wind-stress and the surface pressure, respectively. Terms L_r and D_L are bi- and trilinear
 615 in the model prognostic quantities u, v, p_* , so an on-line computation of the time averages of
 616 the integrands are required for these terms. CAM provides time-mean diagnostic of the zonal
 617 wind u and of the product of the wind components uv conservatively interpolated onto standard
 618 pressure levels, and the integrals in Eq.(A1) are computed with their help.



619 **B Formulation and approximations for the AM correc-** 620 **tion in CAM-FV**

621 The local conservation equation for the shallow-water equations is

$$\begin{aligned} \partial_t [\Delta p (ua \cos \varphi + \Omega a^2 \cos^2 \varphi)] = & \\ & - \frac{1}{a \cos \varphi} \partial_\varphi [\Delta p (ua \cos \varphi + \Omega a^2 \cos^2 \varphi) v \cos \varphi] \quad (\text{A2}) \\ & - \frac{1}{a \cos \varphi} \partial_\lambda [\Delta p (ua \cos \varphi + \Omega a^2 \cos^2 \varphi) u] , \end{aligned}$$

622 where (φ, λ) are latitude and longitude, respectively, Δp is the layer thickness in terms of
 623 hydrostatic pressure, (u, v) are the zonal and meridional wind components, a is the Earth's
 624 radius, and Ω the Earth's angular velocity. Integrating over longitude, we obtain:

$$\int d\lambda \partial_t (\Delta p ua \cos^2 \varphi) = - \int d\lambda \partial_\varphi (\Delta p uv \cos^2 \varphi) + \int d\lambda \Delta p f va \cos^2 \varphi , \quad (\text{A3})$$

625 where f is the Coriolis parameter. To address the FV scheme's violation of this conservation,
 626 we apply an additional, zonally uniform increment of the zonal wind, $\overline{\delta u}$, such that, over each
 627 shallow-water substep δt (we shall refer to this simply as the “time-step” in this section) of the
 628 dynamical core:

$$\begin{aligned} \frac{1}{\delta t} \int d\lambda \cos \varphi [\Delta p_n (u_n + \overline{\delta u}) - \Delta p_o u_o] \cos \varphi = & \\ & - \int d\lambda \cos \varphi \frac{1}{a \cos \varphi} \partial_\varphi (\Delta p uv \cos^2 \varphi) \quad (\text{A4}) \\ & + \int d\lambda \cos^2 \varphi \Delta p f v . \end{aligned}$$

629 Here, “old” prognostic quantities (i.e. valid at the beginning of the time-step) and “new”
 630 prognostic quantities (i.e. valid at the end of the time-step) are indicated by the sub-scripts “o”
 631 and “n”, respectively; quantities without subscripts are intended as time-centred representing
 632 advective fluxes over the time-step. To obtain the correction, we solve this equation for the
 633 required increment $\overline{\delta u}$ and substitute for u_n the actual FV zonal wind increment over the time-
 634 step:

$$u_n = u_o + \left(\xi_o v - \frac{1}{a \cos \varphi} \partial_\lambda K \right) \delta t , \quad (\text{A5})$$



635 where ξ is the absolute vorticity, and K is the kinetic energy term as discretised in LR97's
 636 scheme. The result is:

$$\begin{aligned} \left(\int d\lambda \Delta p_n \right) \overline{\delta u} &= - \int d\lambda \Delta p_n \left(\zeta_o v - \frac{1}{a \cos \varphi} \partial_\lambda K \right) \delta t \\ &\quad - \int d\lambda (\Delta p_n - \Delta p_o) [u_o + (\xi_o v - \zeta_o v) \delta t] \\ &\quad - \int d\lambda \frac{1}{a \cos^2 \varphi} \partial_\varphi (\Delta p uv \cos^2 \varphi) \delta t. \end{aligned} \quad (\text{A6})$$

637 The term in the second line on the right-hand side representing advection of planetary vorticity
 638 is written in a roundabout way for later convenience.

639 We note two aspects of this expression. First, there is a significant numerical cancellation
 640 between the second and the third lines on the right-hand side. Second, all advective terms in
 641 the first two lines on the right-hand side can be easily discretised according to standard LR97's
 642 prescription, and are thus automatically defined on D-grid u-points, i.e. where required for $\overline{\delta u}$.
 643 However, all mass factors are defined on scalar points, i.e. on the A-grid. Furthermore, the
 644 integrand in the third line on the rhs has no natural expression in LR97's discretisation, and
 645 both zonal and meridional winds in that expression need to be interpolated onto the A-grid.
 646 Hence, additional interpolation is required for these terms. Notwithstanding these issues, we
 647 found that this correction, when implemented, gave accurate conservation of AM. However, it
 648 also proved to cause numerical instability, such that the integration crashed within seven or
 649 eight time-steps. Analysis suggested that the last term on the rhs had to be recast in a different
 650 form.

651 We therefore chose to approximate the last term, as follows:

$$\frac{1}{a \cos^2 \varphi} \partial_\varphi (\Delta p uv \cos^2 \varphi) \approx \left[\frac{1}{a \cos \varphi} \partial_\varphi (\Delta p v \cos \varphi) \right] u + \left[\frac{v}{a \cos \varphi} \partial_\varphi (u \cos \varphi) \right] \Delta p. \quad (\text{A7})$$

652 The approximation here consists in using C-grid (advective) fluxes in the partial differentials
 653 on the right-hand side. Considering this as a calculation for the advective fluxes of zonal
 654 momentum, which is its physical meaning, this appears to be a valid interpretation for v . For
 655 the values of Δp and u outside the operators, we adopt the substitutions

$$\begin{aligned} u &=: u_o + \delta_h u + \delta'' u \\ \Delta p &=: \Delta p_n - \delta_h \Delta p + \delta'' \Delta p, \end{aligned}$$

656 where

$$\delta_h \Delta p := \frac{\Delta p_n - \Delta p_o}{2}, \quad \delta_h u := \frac{u_n - u_o}{2}, \quad (\text{A8})$$



657 and $\delta''u$ and $\delta''\Delta p$ are formally $o(\delta t)$. The increments are still understood as advective only, i.e.
 658 they exclude pressure force terms. By further using the identities

$$-\frac{\delta t}{a \cos \varphi} \partial_{\varphi} (\Delta p v \cos \varphi) = \Delta p_n - \Delta p_o + \frac{\delta t}{a \cos \varphi} \partial_{\lambda} (\Delta p u) \quad (\text{A9})$$

$$-\left[\frac{1}{a \cos \varphi} \partial_{\varphi} (u_o \cos \varphi) \right] v \delta t = \left(\zeta_o - \frac{1}{a \cos \varphi} \partial_{\lambda} v_o \right) v \delta t, \quad (\text{A10})$$

659 we finally arrive at the expression for our approximate angular-momentum conserving zonal-
 660 mean zonal wind correction:

$$\begin{aligned} \left(\int d\lambda \Delta p_n \right) \overline{\delta u} &= \int d\lambda (\Delta p_n - \delta_h \Delta p) \left[\frac{1}{a \cos \varphi} \partial_{\lambda} K - \zeta_{\lambda o} v \right] \delta t \\ &+ \int d\lambda \left[\frac{1}{a \cos \varphi} \partial_{\lambda} (\Delta p u) \delta t \right] (u_o + \delta_h u) \\ &+ \int d\lambda \left[2\delta_h \Delta p + \frac{1}{a \cos \varphi} \partial_{\lambda} (\Delta p u) \delta t \right] \delta''u \\ &+ \int d\lambda \delta''\Delta p [\xi_o v - \zeta_{\lambda o} v] \delta t, \end{aligned} \quad (\text{A11})$$

661 where we have used the shorthand $\zeta_{\lambda o} := \frac{1}{a \cos \varphi} \partial_{\lambda} v_o$.

662 We note that setting the higher-order terms to zero implies that the correction has no effect
 663 on a zonally symmetric flow. If, in addition, the flow is in an exact steady-state, then the
 664 correction always vanishes identically, regardless of these terms. It can further be shown that,
 665 if the term in K is the true gradient of the kinetic energy in the original scheme, for any values
 666 of $\delta''u$ and $\delta''\Delta p$ that are first order in δt or higher, the correction (A11) is formally third-order
 667 in δt or higher. In other words, the correction will not affect solutions that are already locally
 668 angular-momentum conserving.

669 In Equation (A11), all mass terms must be averaged over φ ; by contrast, all advective terms
 670 (in square brackets) represent fluxes as discretised according to the standard LR97 algorithm.
 671 The discretised expression of Equation (A11) thus corresponds with Equation (7). The only
 672 additional PPM calculation required to calculate this correction is the meridional advection of
 673 the partial relative vorticity, ζ_{λ} , with a minimal additional computational cost that is hardly
 674 detectable in CAM simulations.



675 C Formulation and implementation of the AM fixer in 676 CAM-FV

677 As we explain in section 2.4, the fixer is based on diagnosing the global change of atmospheric
 678 AM due to advective increments only, which should vanish identically according to the contin-
 679 uous equations. When applies, the fixer counteracts that change at every dynamical sub-step;
 680 irrespectively, its time-mean increments can always be used to diagnose AM non-conservation
 681 in the simulations, in a manner that is completely independent of the physics parametrisations
 682 or boundary conditions used, and hence independent of the particular configuration of the sim-
 683 ulations itself. All the calculations related to the fixer and the quantification of the numerical
 684 (advective) AM source are internal to the dynamical core only, indeed of its shallow-water part.

685 So, for each time-step and at each level k , we require the advective shallow-water equation
 686 increments to satisfy:

$$\delta \left\{ \sum_{i,j} [u_{i,j} \cos e_j + u_{i,j+1} \cos e_{j+1} + a\Omega (\cos^2 e_j + \cos^2 e_{j+1})] \cos c_j \Delta p_{i,j} \right\}_k = 0, \quad (\text{A12})$$

687 where the indices (i, j) refer to longitude and latitude, respectively; e_j are the latitudes of the
 688 u-velocity points of the D-grid; and c_j the latitudes of the scalar points (A-grid). The other
 689 symbols have the same meaning as in the previous section, and δ represent the purely advective
 690 increment obtained in the dynamical core, which may include the correction discussed above.
 691 The action of the fixer in this context is represented by an additional increment $\delta\varpi_k$, so that
 692 the total increment of the zonal wind becomes $\delta u_{i,j,k} + a\delta\varpi_k \cos e_j$. We obtain:

$$\delta\varpi_k = -\frac{T_k}{I_k} \quad (\text{A13})$$

693 where the numerical torque is

$$T_k = a \sum_{i,j} \cos e_j (\cos c_j + \cos c_{j-1}) \{ \delta u_{i,j} \overline{\Delta p_{i,j}^\varphi}(t + \Delta t) + [u_{i,j}(t) + a\Omega \cos e_j] \delta \overline{\Delta p_{i,j}^\varphi} \}_k \quad (\text{A14})$$

694 and the moment of inertia is

$$I_k = a^2 \sum_{i,j} \cos^2 e_j (\cos c_j + \cos c_{j-1}) \overline{\Delta p_{i,j,k}^\varphi}(t + \Delta t). \quad (\text{A15})$$

695 In these expressions,

$$\overline{\Delta p_{i,j,k}^\varphi} := \frac{\Delta p_{i,j,k} \cos c_j + \Delta p_{i,j-1,k} \cos c_{j-1}}{\cos c_j + \cos c_{j-1}}. \quad (\text{A16})$$



696 Equation (A13) gives the required angular acceleration of the entire atmospheric shell at model
697 level k . The action of the “level” fixer is therefore to add an increment to the zonal wind:

$$\delta^f u_{i,j,k} = a \delta \varpi_k \cos e_j. \quad (\text{A17})$$

698 In some regions of the model domain, it is not desirable to apply a fixer, since dissipation is
699 explicitly built into in the dynamical core formulation. This is the case near the upper boundary
700 of CAM’s domain (the lower boundary in pressure space), where the fixer is accordingly switched
701 off. In general, a weight $w_k \leq 1$ can be applied at each level, so that Eq.(A13) becomes

$$\delta \varpi_k = -w_k \frac{T_k}{I_k}, \quad (\text{A18})$$

702 where only a fraction w_k of the numerical torque at level k is compensated by the fixer at that
703 level.

704 The “global” fixer applies the same solid-body rotation increment to all levels within the
705 domain where it is required. When all weights are unity, this is simply

$$\delta \varpi_g = -\frac{\sum_i T_i}{\sum_j I_j}; \quad (\text{A19})$$

706 when $\exists k : w_k < 1$, the vertical integrals must be weighted accordingly, and the weights applied
707 to the correction at each level, so that

$$\delta \varpi_{g,k} = -w_k \frac{\sum_i w_i T_i}{\sum_j w_j I_j}. \quad (\text{A20})$$

708 It can be seen that $\sum_k I_k \delta \varpi_{g,k} = -\sum_k w_k T_k$ so that the numerical torque associated with the
709 domain of interest is fully compensated also by this fixer. Experimentation shew that tapering
710 the global fixer so as to exclude its action from levels in the stratosphere was necessary, in
711 order to avoid distortions of the dynamics in layers where it is sensitive to small amounts of
712 zonal acceleration; and where, moreover, thanks to the predominance of solenoidal dynamics
713 (before gravity-wave drag, which is applied in the physics parametrisations), the dynamical core
714 performs well in terms of AM conservation. For the latter reason, no tapering (i.e. any weights
715 other than 1 in the valid domain, and 0 in the filtered layers near the model lid) is in fact
716 required for the level fixer.

717 For diagnostic purposes, fixer increments are always calculated as in Eq.(A13) and provided
718 in output. Use of the increments in Eq.(A13) lead to conservation of total AM in idealised
719 spin-up or spin-down experiments with no physical sources or sinks of momentum (cf. Figure



720 3), as well as an accurate balance of the surface torques in Held-Suarez or Aquaplanet simu-
721 lations where only surface stresses are present (and accurately diagnosed). Hence, we obtain
722 two important conclusions. First, all numerical sources of AM indeed reside in the advective
723 wind increments of the shallow-water part of the dynamical core; second, the fixer diagnostics
724 return an accurate estimate of the apparent numerical AM source for any CAM-FV integration,
725 irrespective of physics parametrisations or boundary fluxes (including orographic form drag).